THE ASTROPHYSICAL JOURNAL, 351:230–244, 1990 March 1

EVOLUTIONARY VERSUS DYNAMICAL TIME SCALES FOR THE EVOLUTION OF THE CENTRAL STARS OF PLANETARY NEBULAE

J. K. MCCARTHY AND J. R. MOULD
Palomar Observatory, California Institute of Technology
R. H. MENDEZ
Instituto de Astronomia y Fisica del Espacia, Buenos Aires
AND
R. P. KUDRITZKI, D. HUSFELD, A. HERRERO, AND H. G. GROTH
Institut für Astronomie und Astrophysik der Universität München
Received 1989 May 17; accepted 1989 August 31

ABSTRACT

Investigated in this work is the disagreement between evolutionary and dynamical time scales for the evolution of the central stars of planetary nebulae (CSPNs) through the H-R diagram, using the results of high-resolution spectroscopic studies of CSPNs underway at the European Southern Observatory and at Palomar Observatory. These two studies combined have placed 23 CSPN in the distance-independent $\log g - \log T_{\rm eff}$ diagram by comparing their photospheric absorption-line profiles observed at high signal-to-noise ratios with non–LTE (NLTE) model atmosphere line profiles. Results from the new Palomar 1.5 m echelle spectrograph confirm earlier published results from the ESO 3.6 m CASPEC echelle spectrograph for the three CSPNs the two samples have in common. Central star evolutionary ages deduced via comparisons with published evolutionary model calculations are poorly correlated with the dynamical expansion ages for the surrounding nebulae, prompting this investigation.

Three possible reasons for this time scale disagreement are examined: (1) the nebulae could have experienced a phase of rapid photoionization of material ejected previously, while the stars were still on the AGB; (2) the central stars could have undergone a late helium shell flash and returned to the AGB; (3) the AGB–CSPN evolutionary transition times could have been increased by small additional amounts of residual envelope material remaining after the superwind mass-loss phase. While we cannot rule out mechanism (1) as a possible explanation, we find that the so-called born-again mechanism (2) is unlikely for the vast majority of CSPNs in our sample, owing to the very low ratio of dynamical age to interflash period. Our investigation of mechanism (3) demonstrates that the additional residual envelope masses required to reconcile the time scale disagreement are not unreasonable, and we favor this explanation because it is able to account for evolutionary ages both less than and greater than the corresponding dynamical ages. Estimates of residual envelope masses determined empirically as we have done may provide important clues toward an understanding of the AGB star to planetary nebula transition mechanism.

Subject headings: nebulae: planetary — stars: evolution

I. INTRODUCTION

The central stars of planetary nebulae (CSPNs) are an important class of object because they constitute an evolutionary link between the asymptotic giant branch (AGB) and white dwarf stages of stellar evolution. The complete details of the transition from AGB star to planetary nebula are still not understood, although an important piece of this puzzle has been the realization that AGB evolution ends in an "OH/IR star" phase having very strong mass loss, at a rate $\dot{M}$ up to 10^{-4} solar masses per year ($M_\odot$ yr^{-1}; see Knapp *et al.* 1982). The mechanism thought to be responsible for this mass loss is radiation pressure acting on dust which condenses out of the outer atmosphere when gaseous material is carried to large radii by Mira-like pulsations (Wood 1979).

This "superwind" phase (Renzini 1981) causes the OH/IR star to move off the AGB and evolve toward higher effective temperature ($T_{\rm eff}$) as the envelope mass (M_e) and radius decrease at constant luminosity. The pulsations driving the superwind are expected to cease when the envelope mass has decreased to some very small residual amount ($M_{\rm eR}$) of order $10^{-3}\ M_\odot$ (Härm and Schwarzschild 1975), although the exact value of $M_{\rm eR}$ appropriate for a given core mass (M_c) is largely unknown. From an evolutionary point of view, this is most unfortunate, because the residual envelope mass is required to compute the transition time ($t_{\rm tr}$) from the end of the superwind phase to the point at which $T_{\rm eff} = 30{,}000$ K and the CSPN begins to ionize the surrounding neutral material:

$$t_{\rm tr} = (M_{\rm eR} - M_{\rm eN})/\dot{M} \quad (1)$$

(Schönberner 1979; Iben and Renzini 1983), where $M_{\rm eN}$ is the envelope mass at $T_{\rm eff} = 30{,}000$ K and $\dot{M}$ is the net rate at which the envelope mass is being consumed by the combined processes of nuclear burning and mass loss from the surface. Renzini (1981) speculates that "lazy" AGB remnants may exist which have transition times longer than the $\sim$30,000 yr the surrounding ejected AGB envelope takes to disperse. Such "lazy" post–AGB objects would not result in observable planetary nebulae (PNs).

Evolutionary calculations by Schönberner (1979, 1983) and by Wood and Faulkner (1986) trace the evolution of model CSPNs of various masses through the H-R diagram. Evolutionary transition times ($t_{\rm tr}$) along each model track are deter-

mined by assuming that the superwind ceases at some specific temperature, which Schönberner chooses to be between log ($T_{\rm eff}$) = 3.7 and 3.75, and Wood and Faulkner choose to be log ($T_{\rm eff}$) = 3.8. These somewhat arbitrary choices serve to specify $M_{\rm eR}$ as a function of core mass, because for any core mass $T_{\rm eff}$ is a known function of $M_{\rm e}$ (see Fig. 3 of Schönberner 1983). As a result, Schönberner (1983) argues that "*in this scenario there is no room for 'lazy' remnants*," but in our view the matter is far from being settled.

Equally uncertain from a theoretical point of view is the question, During what phase of the AGB star's helium shell flash cycle does PN ejection take place? Iben *et al.* (1983) and Iben (1984) have pointed out that, for PN ejections occurring at phases large enough, it is possible for the next helium shell flash to occur while the post–AGB object is still the central star of a planetary nebula. CSPNs which experience a late helium shell flash then evolve back toward the AGB as a consequence, before resuming their blueward evolution through the H-R diagram. Iben (1984) has suggested on theoretical grounds that perhaps as many as 25% of all planetary nebulae may contain such "born-again" central stars.

Observationally, the study of CSPNs has historically been hampered by the lack of accurate distances to most objects. Statistical distance scales (e.g., Shklovskiĭ 1956; Cahn and Kaler 1971; Acker 1978; Daub 1982) have been invented assuming some parameter (e.g., the ionized mass) of the surrounding planetary nebulae is a constant. The distance scale of Cudworth (1974) is based on proper motions of nearby PNs while Gathier (1984) has determined line-of-sight absorption distances to a sample of PNs. Working from a statistical distance scale, Schönberner (1981) has compared CSPN absolute magnitudes and nebular radii to model evolutionary tracks in the $M_V - t$ diagram, where the times t for all CSPNs follow from the nebular radii and an assumed constant expansion velocity for all the nebulae. Schönberner finds a very narrow mass distribution for CSPNs; in addition to the uncertainties of the distances and variations in expansion velocities, Schönberner's results are also dependent upon the assumption that the *evolutionary* time scales of the central stars can be equated to the *dynamical* expansion time scales of the surrounding nebulae. That this assumption fails when considering individual nebulae and their central stars was pointed out most recently by Mendez *et al.* (1988), and we shall return to this question below in § III of this paper.

In a series of papers, Mendez *et al.* (1981), Mendez, Kudritzki, and Simon (1983, 1985), Mendez *et al.* (1988), and also McCarthy (1988) have studied CSPNs in a distance-independent manner by comparing their photospheric absorption lines observed at high resolution and high signal-to-noise ratios to theoretical NLTE model atmosphere line profiles. This type of analysis allows each CSPN to be placed in the $\log g - \log T_{\rm eff}$ diagram and therein compared to model evolutionary tracks, in order to derive directly the mass of each central star and its age on the evolutionary time scale ($t_{\rm evol}$). We have also shown how it is then possible to derive a spectroscopic distance (Mendez *et al.* 1988; McCarthy 1988) from the best-fit model atmosphere parameters and the observed visual magnitude of the CSPNs. The dynamical expansion age ($t_{\rm dyn}$) of each nebula can be calculated from the spectroscopic distance and the radius and expansion velocity of each particular nebula. We have already pointed out the overwhelming tendency for $t_{\rm dyn}$ to exceed $t_{\rm evol}$ by a large amount for the sample of CSPNs we have studied spectroscopically (Mendez *et al.* 1988), and we have used this fact to argue against the use of the $M_V - t$ diagram for the study of CSPN evolution.

This very significant time scale disagreement is the focus of the present paper, and in § IV below we examine three possible explanations and discuss the implications of the one we find most convincing. But first, we summarize in § II the observational material and the NLTE model atmosphere fitting process on which our time scale determinations are based, and in § III we review the time scale calculations in order to quantify the time scale disagreement.

II. THE OBSERVATIONAL MATERIAL

This investigation is based on the results of our high-resolution spectroscopic studies of CSPNs underway at the European Southern Observatory (Mendez *et al.* 1988) and at Palomar Observatory (McCarthy 1988). Our combined sample includes the 23 CSPNs listed in the first column of Table 1. We have observed these CSPNs at resolutions typical of Cassegrain echelle spectrographs: $R = \lambda/\Delta\lambda \sim 40{,}000$ per pixel with the Palomar 1.5 m echelle spectrograph (see McCarthy 1988) and $\sim 30{,}000$ per pixel with the ESO 3.6 m CASPEC spectrograph (see le Luyer, Melnick, and Richter 1979; D'Odorico *et al.* 1983); the instrumental FWHM being roughly 2 pixels in each case. The wavelength range we selected with CASPEC covers from 4100 to 5000 Å, while the Palomar 1.5 m echelle covers the range from $\lambda_{\rm min} \lesssim 4000$ Å to $\lambda_{\rm max} > 7000$ Å, owing to the use of prism cross-dispersion elements and a larger format (800 × 800 pixel) Texas Instruments CCD. We require high signal-to-noise ratios (S/N ~ 80–100 or more) for the subsequent analysis of the reduced data, in which we compare each central star's photospheric hydrogen and helium line profiles to NLTE model atmosphere line profiles (Kudritzki and Mendez 1989, and references therein; especially Herrero 1987*a*, *b*).

The result of these detailed comparisons is a simultaneous fit to the CSPN photospheric hydrogen and helium line profiles for a single set of NLTE model atmosphere parameters: effective temperature $T_{\rm eff}$, surface gravity $\log g$, and photospheric helium abundance by number y. We believe that conservative error estimates for these best-fit atmospheric parameters are as follows: $\pm 10\%$ in $T_{\rm eff}$, ± 0.2 in $\log g$, and $\pm 20\%$ in y (Mendez *et al.* 1988; Kudritzki and Mendez 1989). Although we have demonstrated (McCarthy 1988) that the formal errors from the noise in the observed spectra are typically a factor of 2 less than these quoted estimates, it is possible that uncertainties in the NLTE model atmosphere and line formation calculations enter at this level also.

We should point out that our initial fit results from the Palomar 1.5 m echelle spectrograph (McCarthy 1988) agree well with our earlier fit results (Mendez *et al.* 1988) using the ESO 3.6 m CASPEC echelle spectrograph for the three CSPNs the northern and southern hemisphere samples have in common (NGC 1360, NGC 2392, and NGC 4361). In no case did the two fit results differ by an amount greater than the quoted errors, and the most serious disagreement was a $\log g$ difference of 0.2 in the case of NGC 2392 (3.8 as opposed to 3.6; McCarthy 1988). This difference may be attributed to the slightly higher resolution of the Palomar 1.5 m echelle spectrograph compared to CASPEC, leading to less filling in of the CSPN absorption-line cores by nebular emission. But given the excellent agreement in the cases of NGC 1360 and NGC 4361, we feel that a more likely explanation is filling in of the NGC 2392 line profile cores by intrinsically variable stellar

TABLE 1

EVOLUTIONARY AND DYNAMICAL PROPERTIES OF CSPNs

Object Name (1)	$T_{\rm eff}$ (K) (2)	log g (cgs) (3)	M ($M_\odot$) (4)	$t_{\rm evol}$ (10^3 yr) (5)	$t_{\rm dyn}$ (10^3 yr) (6)	$t_{\rm dyn} - t_{\rm evol}$ (10^3 yr) (7)	$M_{\rm eR_0}$ ($M_\odot$) (8)	dM_e/dt ($M_\odot$ yr^{-1}) (9)	$M'_{\rm eR}$ ($M_\odot$) (10)
NGC 7293	90,000	6.9	0.546	396.	39.0	−357.	5.13×10^{-3}	...[a]	4.17×10^{-4}
NGC 1360[b]	$75{,}000^{+7500}_{-7500}$	$5.5^{+0.2}_{-0.2}$	$0.547^{+0.002}_{-0.001}$	$135.^{+120}_{-80}$	$17.8^{+4.6}_{-3.6}$	$-117.^{+80}_{-120}$	$4.87^{+0.26}_{-0.95} \times 10^{-3}$	...[a]	$1.91^{+0.77}_{-0.60} \times 10^{-3}$
NGC 4361[b]	$80{,}000^{+8000}_{-8000}$	$5.4^{+0.2}_{-0.2}$	$0.553^{+0.01}_{-0.004}$	38.0^{+51}_{-23}	$22.0^{+3.4}_{-2.7}$	-16.0^{+23}_{-51}	$2.77^{+1.13}_{-1.16} \times 10^{-3}$	...[a]	$1.35^{+0.22}_{-0.17} \times 10^{-3}$
IC 2448	65,000	4.8	0.571	8.40	7.0	−1.40	1.23×10^{-3}	...[a]	1.10×10^{-3}
LSE 125	85,000	5.1	0.612	3.16	22.0	18.8	7.67×10^{-4}	4.55×10^{-8}	1.62×10^{3}
A 36[b]	$95{,}000^{+9500}_{-8500}$	$5.3^{+0.2}_{-0.2}$	$0.613^{+0.04}_{-0.03}$	$3.25^{+1.2}_{-0.24}$	$22.8^{+6.6}_{-5.0}$	$19.6^{+6.6}_{-5.1}$	$7.57^{+2.21}_{-2.61} \times 10^{-4}$	$4.60^{+1.91}_{-2.61} \times 10^{-8}$	$1.66^{+0.57}_{-0.27} \times 10^{-3}$
NGC 1535	70,000	4.6	0.668	1.44	6.0	4.56	4.34×10^{-4}	7.33×10^{-8}	7.69×10^{-4}
NGC 3242	75,000	4.7	0.675	1.68	4.0	2.32	4.16×10^{-4}	7.63×10^{-8}	5.93×10^{-4}
H 2-1	33,000	3.3	0.680	0.70	5.0	4.30	4.03×10^{-4}	7.86×10^{-8}	7.41×10^{-4}
He 2-162	27,000	2.9	0.680	1.06	6.0	4.94	4.04×10^{-4}	7.84×10^{-8}	7.92×10^{-4}
IC 4637	50,000	4.0	0.692	1.31	3.0	1.69	3.80×10^{-4}	8.30×10^{-8}	5.20×10^{-4}
NGC 7009	82,000	4.8	0.699	1.74	7.0	5.26	3.65×10^{-4}	8.60×10^{-8}	8.17×10^{-4}
He 2-182	36,000	3.4	0.721	1.23	2.0	0.077	3.19×10^{-4}	9.53×10^{-8}	3.92×10^{-4}
He 2-151	25,000	2.7	0.730	0.71	14.0	13.3	2.99×10^{-4}	9.97×10^{-8}	1.62×10^{-3}
M 1-26	33,000	3.2	0.762	1.00	2.0	1.00	2.36×10^{-4}	1.17×10^{-7}	3.53×10^{-4}
Tc 1	33,000	3.2	0.762	1.00	11.0	10.0	2.36×10^{-4}	1.17×10^{-7}	1.40×10^{-3}
NGC 6629	47,000	3.8	0.767	0.98	29.0	28.0	2.28×10^{-4}	1.19×10^{-7}	3.58×10^{-3}
NGC 2392[b]	$47{,}000^{+5000}_{-5000}$	$3.8^{+0.2}_{-0.2}$	$0.767^{+0.10}_{-0.03}$	$0.98^{+0.90}_{-0.38}$	$1.2^{+0.4}_{-0.3}$	$0.22^{0.55}_{-0.95}$	$2.28^{+0.05}_{-0.13} \times 10^{-4}$	$1.19^{+0.05}_{-0.13} \times 10^{-7}$	$2.54^{+0.50}_{-0.79} \times 10^{-4}$
NGC 6891	50,000	3.9	0.768	0.93	12.0	11.1	2.27×10^{-4}	1.20×10^{-7}	1.55×10^{-4}
NGC 6210[b]	$50{,}000^{+5000}_{-5000}$	$3.9^{+0.2}_{-0.2}$	$0.768^{+0.10}_{-0.04}$	$0.93^{+0.90}_{-0.36}$	$8.8^{+3.5}_{-3.1}$	$7.87^{+3.5}_{-3.1}$	$2.27^{+0.05}_{-0.13} \times 10^{-4}$	$1.20^{+0.05}_{-0.01} \times 10^{-3}$	$1.17^{+0.34}_{-0.27} \times 10^{-3}$
IC 418	36,000	3.3	0.818	0.44	6.0	5.56	1.68×10^{-4}	1.52×10^{-7}	1.01×10^{-3}
He 2-108	33,000	3.1	0.873	0.15	36.0	35.9	1.58×10^{-4}	1.88×10^{-7}	6.91×10^{-3}
He 2-138	27,000	2.7	0.870	0.92	8.0	7.08	1.57×10^{-4}	1.86×10^{-7}	1.47×10^{-3}

[a] For objects having $t_{\rm evol} > t_{\rm dyn}$, $M'_{\rm eR}$ was determined directly from the evolutionary models using eq. (8) of the text and not calculated on the basis of eq. (4) of the text.

[b] These five CSPNs were observed with the new Palomar 1.5 m echelle spectrograph (McCarthy 1988).

wind emission. Therefore we conclude that these initial Palomar 1.5 m echelle spectrograph results confirm our earlier published CASPEC results (Mendez *et al.* 1988) and demonstrate how reliable propertly reduced echelle data are for this type of NLTE line profile analysis.

Finally, the best-fit NLTE model atmosphere parameters allow us to place the CSPN in the distance-independent log g − log $T_{\rm eff}$ plane and therein compare them to theoretical evolutionary models. In this manner, it is possible for us to derive estimates of the central star masses ($\simeq M_c$) and post–AGB ages ($t_{\rm evol}$) on the evolutionary time scale of the models. For this purpose, we have employed the evolutionary models of Schönberner (1979, 1983) for central star masses 0.546, 0.565, 0.598, and 0.644 $M_\odot$, and the Wood and Faulkner (1986) type A mass-loss models with masses 0.70, 0.76, and 0.89 $M_\odot$. We refer the interested reader to Mendez *et al.* (1988) or McCarthy (1988) for a thorough discussion of the NLTE model atmosphere analysis, the errors involved, and the resulting distribution of CSPNs in the log g − log $T_{\rm eff}$ plane.

III. TIME SCALE CALCULATIONS

a) $t_{\rm evol}$

We compute the age $t_{\rm evol}$ of each CSPN on the evolutionary time scale by interpolating between published models of Schönberner (1979, 1983) and Wood and Faulkner (1986). Note, however, that Schönberner defines the zero point of his evolutionary time scale ($t_{\rm evol,\,S} = 0$) to correspond to the point at which the post–AGB model reaches log $T_{\rm eff} = 3.75$, whereas Wood and Faulkner define the zero point of their evolutionary time scale ($t_{\rm evol,\,WF} = 0$) to correspond to log $T_{\rm eff} = 4.00$; the first model point for which they publish data has log $T_{\rm eff} = 3.80$ and $t_{\rm evol,\,WF} < 0$ (see the end of the superwind phase discussed in § I above).

In order to make use of both sets of models—which cover different mass ranges as pointed out above—in a self-consistent manner, we have transformed each of the models onto a common time scale having its zero point ($t_{\rm evol} = 0$) corresponding to log $T_{\rm eff} = 3.80$. In the case of the Wood and Faulkner (1986) type A mass-loss models, this was relatively straightforward; the difference between $t_{\rm evol,\,WF}$ at log $T_{\rm eff} = 4.00$ and log $T_{\rm eff} = 3.80$ could be read from Wood and Faulkner's Table 1 and added to the values of $t_{\rm evol,\,WF}$ tabulated for each model. In the case of the Schönberner (1979, 1983) models, the difference between $t_{\rm evol,\,S}$ at log $T_{\rm eff} = 3.80$ and log $T_{\rm eff} = 3.75$ had to be determined first by interpolation between the time steps as taken from a plot of the evolutionary track and then subtracted from the $t_{\rm evol,\,S}$ values measured along each track.

To determine $t_{\rm evol}$ for each CSPN in our sample, the age of each model track at the best-fit $T_{\rm eff}$ was first determined by interpolation along that track. The final step was to interpolate between this set of ages as a function of log g to find the CSPN evolutionary age $t_{\rm evol}$ corresponding to the best-fit log g. The results of this calculation are given in column (5) of Table 1. Errors in $t_{\rm evol}$ resulting from errors of ±10% in $T_{\rm eff}$ and ±0.2 in log g are provided in Table 1 for the five CSPNs we have studied from Palomar (McCarthy 1988); these errors are to be understood as representative of the corresponding uncertainties in the remaining objects (Mendez *et al.* 1988). In the

three cases of overlap between the two samples, we have used the Palomar results (with errors) in place of the CASPEC results in order to avoid double-counting of these objects.

b) t_{dyn}

We determined the dynamical expansion age t_{dyn} for each planetary nebula in the customary manner from the ratio of the linear radius of the nebular shell to the shell's expansion velocity (v_{exp}). The linear radius was derived from the angular radius of the nebular shell and the distance to the object. Errors in the linear radius are dominated by errors in the distance; we find that the spectroscopic distances we have determined from our best-fit model atmospheres and the visual magnitudes of the CSPNs are among the most reliable distance estimates available. We have previously estimated (Mendez *et al.* 1988; McCarthy 1988) that typical errors in our spectroscopic distances are between 20% and 30% and that these errors are dominated by the errors in determining log g for each CSPN. Although the errors in measuring angular radii were not nearly as large, we do overestimate t_{dyn} slightly by having used shell outer radii instead of inner radii. Recall that t_{evol} represents an age from the *end* of the superwind phase, and we would prefer t_{dyn} to conform to this definition as much as possible. Unfortunately, inner radii have not been measured in any standardized manner and were thus unavailable for the present purpose. The outer radii adopted are from Wilson (1950), Westerlund and Henize (1967), and Acker *et al.* (1982).

We have used our measured expansion velocities for the nebular shells from our CASPEC spectrograms (Mendez *et al.* 1988). For the Palomar data, we have adopted values of v_{exp} determined by Wilson (1950) and Bohuski and Smith (1974), except in the case of NGC 4361, for which we have measured a value of $v_{exp} = 27.7$ km s^{-1} from our Palomar 1.5 m echelle spectrogram (McCarthy 1988), after having found discrepant values in the literature.

The resulting dynamical ages can be found in column (6) of Table 1. As before, we have provided error estimates for the five CSPNs studied from Palomar, but possible errors resulting from the use of outer radii rather than inner radii are not included in these estimates. We have previously pointed out (Mendez *et al.* 1988) that using inner radii would possibly reduce t_{dyn} by as much as a factor of 3, because the observed ratio of inner to outer nebular radii (see Taylor, Pottasch, and Zhang 1987) is frequently as low as 0.3 for some nebulae such as IC 418; for young, high-surface brightness nebulae, however, the shells are believed to be very thin (e.g., NGC 7027; Masson 1989), and much less error has been introduced by the use of outer radii in place of inner radii.

c) Comparison

The lack of agreement between the dynamical expansion ages and the evolutionary ages can be seen most clearly from Figure 1, which shows t_{dyn} plotted as a function of t_{evol}. The diagonal line through this figure represents $t_{dyn} = t_{evol}$. The fact that most CSPNs lie above and to the left of this line indicates a trend in our sample toward "old" nebulae around "young" central stars.

Note that the ratios of dynamical to evolutionary ages are often very large (up to factors of 30 or more in some cases). This difference is much too large to be accounted for only in terms of known observational uncertainties (e.g., distances and our use of outer instead of inner radii). Therefore we conclude that the disagreement between t_{dyn} and t_{evol} is a real consequence of the evolution of planetary nebulae and their central stars which needs to be investigated and explained.

Finally, note that the sense in which t_{dyn} and t_{evol} differ in our

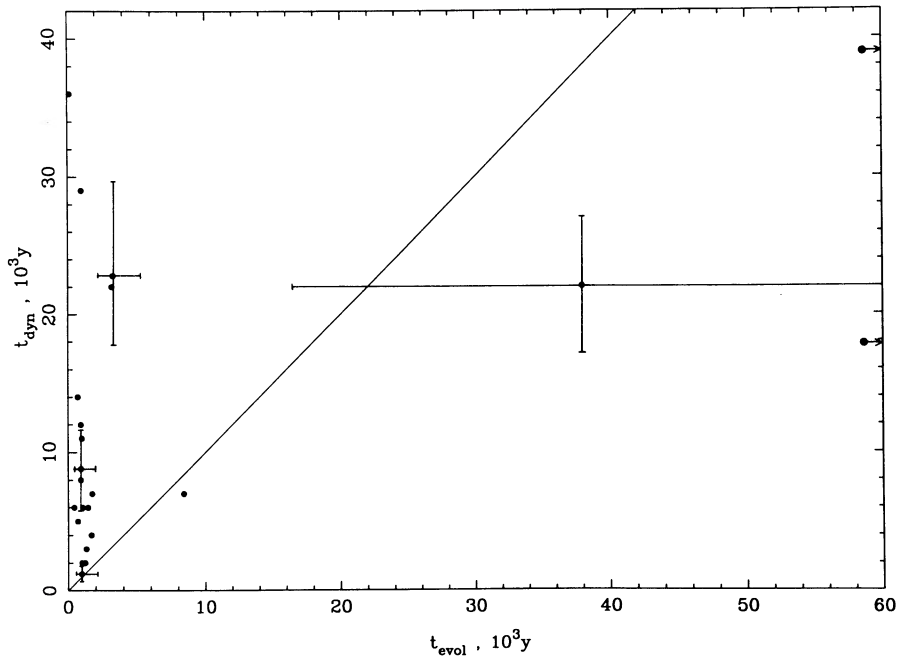

FIG. 1.—Plot of dynamical ages of the surrounding planetary nebulae (derived assuming constant expansion velocity) vs. evolutionary ages for the central stars of those nebulae (derived via comparisons to evolutionary models in the log g − log T_{eff} plane). The four error bars on objects from McCarthy (1988) are representative of errors expected for the remaining objects (Mendez *et al.* 1988) in our combined sample. Note the predominance of "old" nebulae surrounding "young" central stars.

sample—"old" nebulae around "young" central stars—is exactly the opposite sense of that noted by Gathier (1984) for his (much different) sample of CSPNs. Taken at face value, the distance estimates Gathier derived imply that his sample of CSPNs is dominated by low-luminosity and therefore low-mass objects. Based on the evolutionary time scale of Schönberner (1979, 1983), these central stars would be many times *older* than their surrounding planetary nebulae. While there is reason to doubt some of the distances compiled by Gathier (see Mendez *et al.* 1988), the low-mass CSPNs in our sample (NGC 1360, NGC 4361, and NGC 7293 in Table 1) share the time scale disagreement in the same sense as noted by Gathier (1984). We will return to these objects in our discussion of possible explanations at the close of § IV below, because they provide a valuable contrast to the bulk of our sample.

IV. POSSIBLE EXPLANATIONS

There are in general three ways in which the disagreement between dynamical expansion ages and evolutionary ages for the young CSPNs shown in Figure 1 can be reconciled. (1) The ionized nebulae could have reached their present sizes in much shorter times than those derived on the basis of their present radii and their respective expansion velocities; such would be the case if the nebulae experienced a phase of rapid photoionization of material ejected previously, in a stellar wind while the stars were still on the AGB. (2) The actual evolutionary ages could be much longer than those calculated on the basis of evolutionary models for CSPN evolution; such would be the case if the central stars have experienced a late helium shell flash and as a result evolved back toward the AGB. (3) The predicted transition times could be too short, and thus the two time scales may not share the same zero point; such would be the case if the superwind ceases at a slightly lower temperature than log $T_{\rm eff} = 3.80$ (or 3.75), increasing the transition time given by equation (1) by leaving a small additional amount of residual envelope mass on the surface of the remnant. These three possibilities will be examined in turn below, beginning with the rate of expansion of the ionized nebulae.

a) Rapid Photoionization of an AGB Envelope

Given that "young" CSPNs are thought to be surrounded by the neutral material ejected during the prior OH/IR star phase of evolution—which should extend out to large distances from the central star—one is led to ask the question of whether the expansion of the ionized nebulae must be restricted to only the $v_{\rm exp}$ measured radially along the line of sight (i.e., the bulk motion of the ionized gas). Note that the size of the visible nebula is determined by the radius of an *ionization front*, and it is conceivable that during the early evolution of the nebula, this ionization front could have expanded into the surrounding neutral material at a much more rapid pace than the material itself was expanding.

In order to investigate this question in greater detail, we developed a computer model to simulate the photoionization of material ejected by an AGB star superwind as the star evolves into a CSPN along a Schönberner (1983) or Wood and Faulkner (1986) evolutionary track. Making the simplifying assumptions that (i) the superwind mass-loss rate, $\dot{M}$, and ejection velocity, $V_{\rm ej}(r) = V_0(r/R_0)^{\beta}$, are constant with time prior to $t_{\rm evol} = 0$; (ii) the CSPN emits ionizing radiation ($\nu > \nu_{\rm L}$, the Lyman limit) with a blackbody spectrum; and (iii) ignoring absorption of Lyman continuum photons by dust, we derive the following differential equation for the rate of change of the Strömgren (1939) radius, r_s, with time:

$$\frac{dr_s}{dt} = \frac{1}{4\pi r_s^2 n_0}\left(\frac{r_s}{R_0}\right)^{\beta+2}\left\{4\pi R_*^2 \frac{2\pi k T_*}{hc^2}\nu_{\rm L}^2 e^{-h\nu_{\rm L}/kT_*} - \frac{4\pi}{(2\beta+1)} n_0^2 \alpha^{(2)} R_0^3\left[\left(\frac{R_i}{R_0}\right)^{-(2\beta+1)} - \left(\frac{r_s}{R_0}\right)^{-(2\beta+1)}\right]\right\} \quad (2)$$

(McCarthy 1988). In equation (2), radii are normalized in terms of R_0, the AGB star radius at $t_{\rm evol} = 0$ (see the above normalization of $V_{\rm ej}$ as a function of radius. R_* is the actual radius of the star, which decreases as the star evolves, while R_i is the inner radius of the ejected proto–planetary nebula shell, which increases with time as the ejected material moves away from the star at a rate $V_{\rm ej}$. The density distribution was determined from the above velocity law assuming conservation of mass, so that $n(r) = n_0(r/R_0)^{-(\beta+2)}$, where the factor n_0 can be expressed in terms of the AGB mass-loss rate $\dot{M}$ and the mass $m_{\rm H}$ of the hydrogen atom as $n_0 = \dot{M}/(4\pi R_0^2 m_{\rm H} V_0)$. The factor $\alpha^{(2)}$ in equation (2) is the recombination coefficient to all energy levels of hydrogen above the second (i.e., recombinations directly into the $n = 1$ state will emit Lyman continuum photons which are capable of ionizing another hydrogen atom nearby in the nebula), and its numerical value was taken from Spitzer (1978) for a temperature of 10^4 K in the ionized region. The remaining factors k and h are the Boltzmann and Planck constants, respectively.

Given (i) the input parameters $\dot{M}$, V_0, β, and R_0 pertaining to the AGB superwind mass loss and (ii) the time-dependent input functions $T_{\rm eff}(t)$ and $R_*(t) \propto L_*^{1/2}(t)T_{\rm eff}^{-2}(t)$ from the CSPN evolutionary model adopted, equation (2) could be solved via the Runge-Kutta method to determine the Strömgren radius r_s as a function of time. The results for a 0.6 $M_\odot$ CSPN are shown in Figure 2, where $\dot{M} = 3 \times 10^{-5}$ $M_\odot$ yr^{-1}, $V_0 = 15$ km s^{-1}, $\beta = 0$, and $R_0 = 100$ $R_\odot$ (the radius the 0.6 $M_\odot$ Schönberner CSPN model has at $t_{\rm evol} = 0$). Notice that the Strömgren radius, given in parsecs as a function of time by the solid line in Figure 2, increases linearly at first for $t_{\rm evol} \geq 0$. During this phase the ionized mass, given in units of $M_\odot$ by the dotted line in Figure 2, remains very small; the Strömgren radius is merely following the linear growth of R_i with time as the AGB envelope expands with $V_{\rm ej} = V_0$. But then when $T_{\rm eff}$ for the central star, given in units of 10^5 K by the dashed line in Figure 2, reaches roughly 30,000 K at $t_{\rm evol} \sim 3000$ yr, it emits enough ionizing photons to increase r_s beyond the inner radius R_i of the expanding shell, and thus the Strömgren radius increases at a rate larger than $V_{\rm ej}$ and the ionized mass increases to some nonzero amount as well. The very rapid rate at which the ionized radius expands (i.e., the large dr_s/dt) can be attributed to the $1/r^2$ density distribution surrounding the CSPN, because both a constant mass-loss rate $\dot{M}$ and a constant ejection velocity ($\beta = 0$) have been assumed. Figures 3, 4, and 5 show the results of increasing the mass-loss rate to $\dot{M} = 5 \times 10^{-5}$, 1×10^{-4}, and 2×10^{-4} $M_\odot$ yr^{-1}, respectively. Figures 2–5 are representative of the range of mass-loss rates determined from molecular CO densities in OH/IR star envelopes (Knapp *et al.* 1982); as expected, the ionization of the AGB envelope is delayed as the density increases, but dr_s/dt still greatly surpasses $V_{\rm ej}$ for $t_{\rm evol} \geq 3000$ yr and $\dot{M} < 1 \times 10^{-4}$ $M_\odot$ yr^{-1}. In the two highest density cases, the recombination rate is actually large enough that the decrease in the number of ionizing photons for $T_{\rm eff} > 75{,}000$ K ($t_{\rm evol} \geq 6000$ yr) causes the Strömgren radius (e.g., the solid line in Fig. 4) and ionized

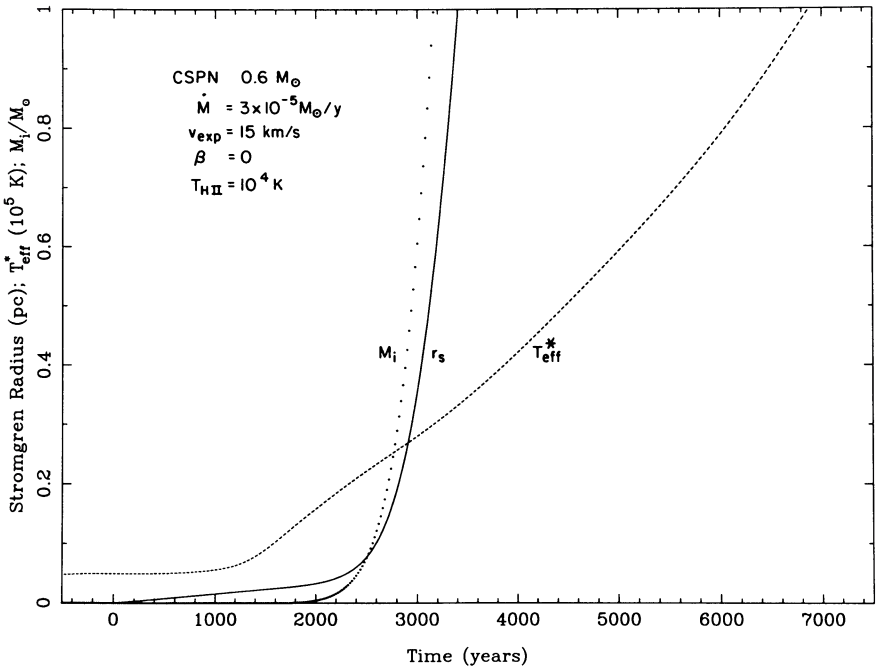

FIG. 2.—Growth with time of the Strömgren radius of a model AGB envelope (solid line, units are parsecs), ejected with a mass-loss rate of $3 \times 10^{-5}\ M_{\odot}\ \mathrm{yr}^{-1}$ and ejection velocity 15 km s^{-1}, around a 0.6 $M_{\odot}$ central ionizing source (T_{eff} given by dashed line, units are 10^5 K; Schönberner 1983). Dotted line shows the time rate of change of the ionized mass in units of $M_{\odot}$.

mass (e.g., the dotted line in Fig. 5) to decrease significantly as well.

Note, however, that the rapid increase of the Strömgren radius shown in these figures will continue only until reaching the outer radius of the material lost by the AGB star (not shown); for a main-sequence progenitor mass of 1.2 $M_{\odot}$ and a CSPN core mass of 0.6 $M_{\odot}$, the ionized mass of the PN shell (M_{is}) obviously cannot exceed 0.6 $M_{\odot}$. The model Strömgren radius presented in Figure 2 has already surpassed 1 pc before this amount of AGB envelope material is ionized (recall that it was the lowest density example). For the model in Figure 4, however, the finite envelope mass will cause the Strömgren radius to stop increasing rapidly upon reaching a radius $r_s \sim 0.15$ pc (for $M_{\mathrm{is}} = 0.6\ M_{\odot}$); for later t_{evol}, the Strömgren radius will continue to expand linearly with time at a rate $\sim V_{\mathrm{ej}}$.

Analogous envelope ionization calculations were also per-

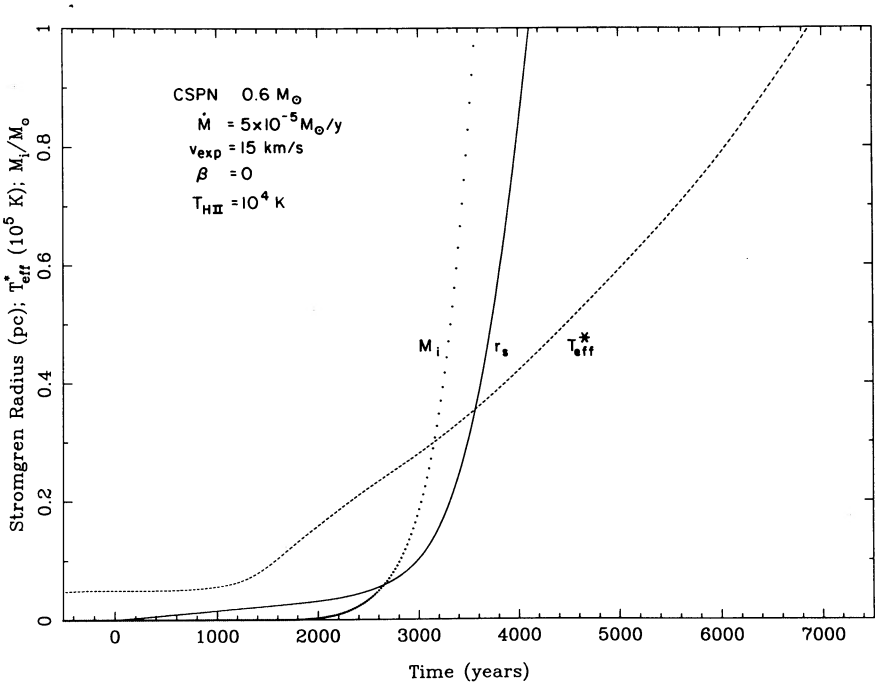

FIG. 3.—Same as Fig. 2, but with a higher AGB mass-loss rate of $5 \times 10^{-5}\ M_{\odot}\ \mathrm{yr}^{-1}$

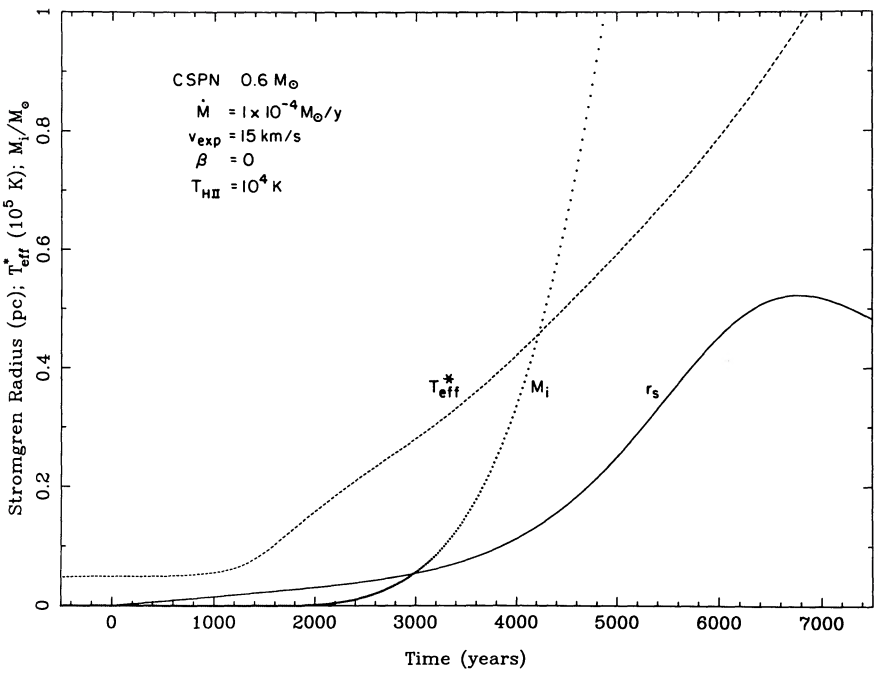

FIG. 4.—Same as Fig. 2, but with a higher AGB mass-loss rate of $1 \times 10^{-4} M_{\odot}$ yr^{-1}

formed for CSPN masses of 0.565, 0.70, 0.76, and 0.89 $M_{\odot}$ over similar ranges of $\dot{M}$ (see McCarthy 1988, Figs. 4-21–4-29 for complete details). The 0.565 and 0.70 $M_{\odot}$ cases were qualitatively similar to the 0.6 $M_{\odot}$ results discussed above; the less rapid increase in $T_{\rm eff}$ as a function of time in the 0.565 $M_{\odot}$ case delayed somewhat the ionization of the surrounding envelope, especially at high values of $\dot{M}$, while the reverse is true in the 0.70, 0.76, and 0.89 $M_{\odot}$ cases. Each of the three more massive CSPNs evolve to higher effective temperatures at higher luminosities, which enables them to ionize the surrounding envelope sooner than the 0.6 $M_{\odot}$ CSPN, but the subsequent decline in the number of ionizing photons also occurs more rapidly. In the most extreme of the calculations performed (CSPN mass 0.89 $M_{\odot}$, $\dot{M} = 5 \times 10^{-5} M_{\odot}$ yr^{-1}; see Fig. 4-29 of McCarthy 1988), the significant ionization beyond the inner edge of the shell only lasts from $t_{\rm evol} = 500$ yr to $t_{\rm evol} = 700$ yr, although it was possible in this brief period to ionize over 0.7 $M_{\odot}$ of the surrounding AGB envelope ejecta.

The results of these numerical experiments simulating the photoionization of an ejected AGB envelope do indeed suggest

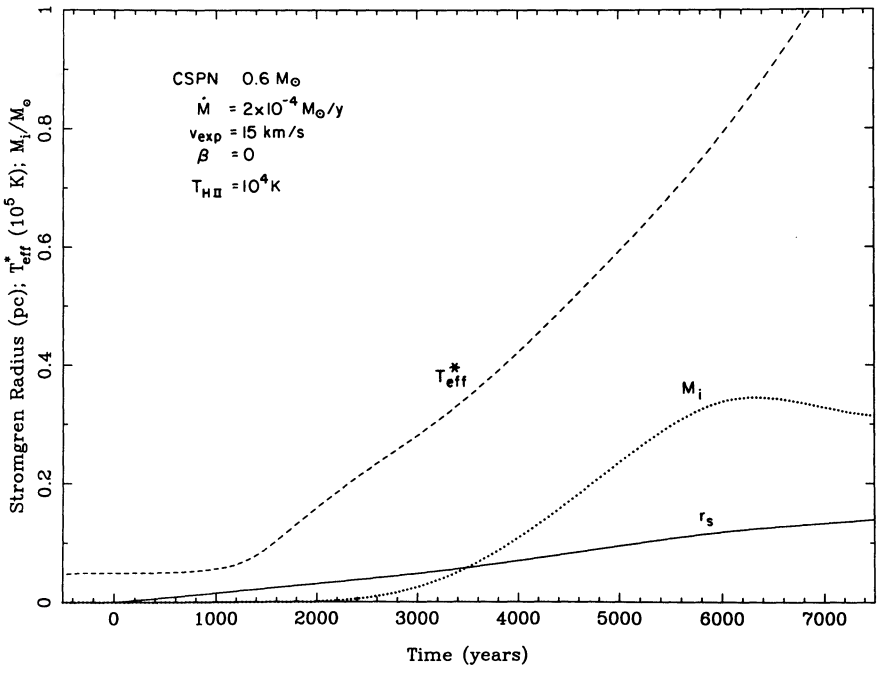

FIG. 5.—Same as Fig. 2, but with a higher AGB mass-loss rate of $2 \times 10^{-4} M_{\odot}$ yr^{-1}

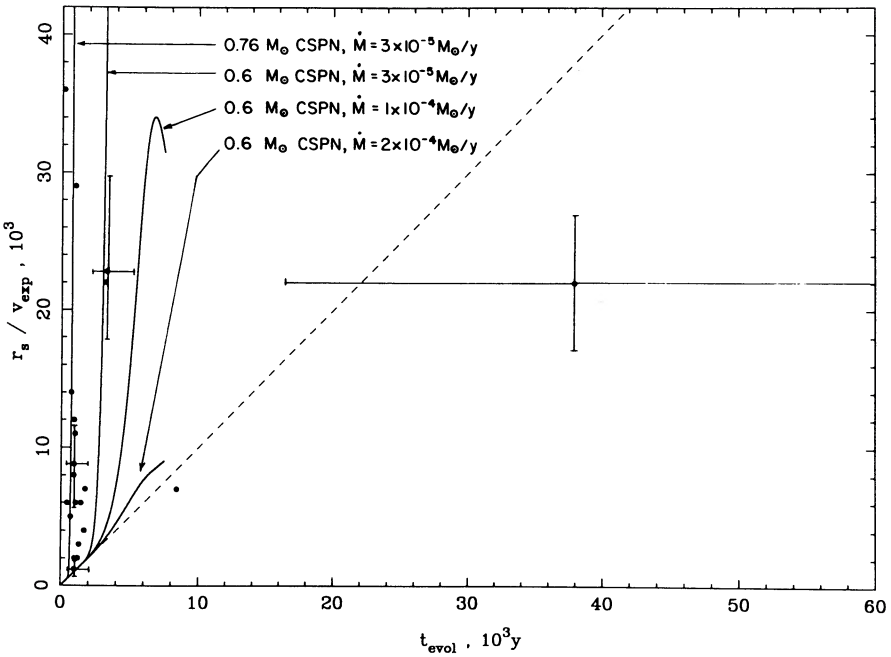

FIG. 6.—The "dynamical ages" (r_s/v_{exp}) one would derive as a function of "evolutionary" time for models analogous to Fig. 2, compared to the observational data shown also in Fig. 1.

that the expansion rate of the ionization front can exceed that of the bulk material. The implications of this result for the t_{evol} versus t_{dyn} time scale disagreement of Figure 1 can be seen in Figure 6, in which the data points of Figure 1 are compared with the $t_{dyn} = r_s/v_{exp}$ curves one would derive if real planetary nebulae behaved like the photoionization models presented in § IV*a* above. Clearly the behavior of the models is capable of resolving the disagreement between the t_{evol} and t_{dyn} age estimates. The question then becomes, To what extent do our simple photoionization models resemble real planetary nebulae? We will return to this question in § IV*d* below after considering two alternate ways the disagreement between t_{evol} and t_{dyn} can be explained: the t_{evol} ages are incorrect as a result of a late He shell flash or else do not share the same zero point as the t_{dyn} ages, owing to our lack of understanding of the cessation of the superwind mass-loss phase.

b) Late He *Shell Flash*

Regarding the alternate possibility (2) that the theoretical evolutionary times are in error, Iben *et al.* (1983) and Iben (1984) have suggested that, as a result of a late helium shell flash experienced during the planetary nebula phase, it is possible for CSPNs to evolve back toward the AGB. The CSPNs subsequently retrace their earlier evolutionary tracks toward higher temperatures before finally cooling to become white dwarfs. Such "born-again" CSPNs would in fact be older than our t_{evol} ages suggest, since they are evolving away from the AGB for the second time, not the first as we have assumed when deriving t_{evol} from the Schönberner (1983) or Wood and Faulkner (1986) evolutionary tracks.

We have decided to investigate this possibility by plotting (see Fig. 7) as a function of CSPN core mass the ratio of the interflash period Δt_{flash} between successive He shell flashes (Paczyński, 1975; Schönberner, 1979) to the dynamical age t_{dyn} of the surrounding nebula for each object in our combined sample. The dashed horizontal line through the diagram corresponds to a dynamical age equal to the evolutionary time period between helium shell flashes. Since none of the CSPNs in our sample lie above this line, we do not find any obvious candidates for "born-again" evolution, especially in light of the suggestion by some theorists that PN ejection is more likely at the luminosity peak of the shell flash period (e.g., Schönberner 1983); were this the case, the next such flash would occur at $t_{dyn} = \Delta t_{flash}$ and $t_{dyn}/\Delta t_{flash}$ ratios greater than unity in Figure 7 would be expected for postflash "born-again" CSPNs. No such objects appear in the present sample, although it is perhaps too small and contains too few low-mass CSPNs to draw any definite conclusions.

Future work should nevertheless investigate in greater detail the uppermost objects (NGC 7293, NGC 1360, and NGC 4361) in Figure 7 for additional evidence for or against the "born-again" hypothesis. Such an investigation is outside the scope of the present discussion; we wish to point out, however, that for these three particular low-mass CSPNs, t_{evol} exceeds t_{dyn} in Table 1 already, and so the time scale disagreement would become even worse were the "born-again" mechanism to increase t_{evol} by some additional amount. Therefore, we must look elsewhere to explain the time scale disagreement for these three objects, because not only the late He shell flash but also the rapid nebulae photoionization phenomena are unable to explain values of t_{evol} many times greater than t_{dyn}. In § IV*d* below, we shall discuss the implications of Figure 7 for time scale disagreement of the majority of objects in our present sample, those with t_{evol} values less than t_{dyn}.

c) Empirical Residual Envelope Masses

Turning finally to possibility (3) concerning the zero points of the two time scales, t_{evol} and t_{dyn}, we shall assume here that $t_{dyn} = 0$ corresponds to the end of the "superwind" mass-loss phase which occurs at the tip of the AGB to produce an expanding planetary nebula and that our derived values of t_{dyn} reflect the time elapsed since this occurrence (see § IV*a* above,

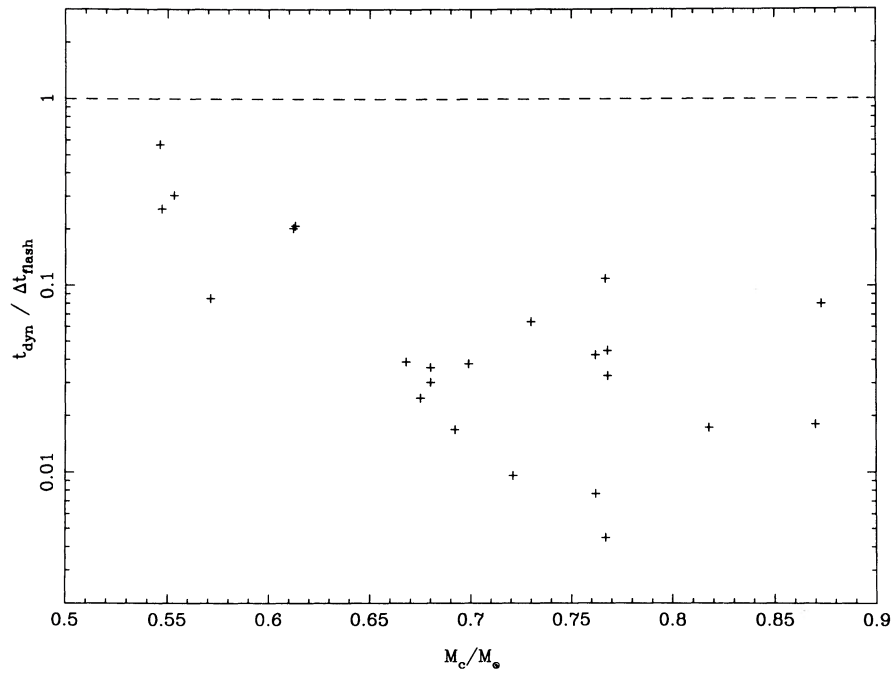

FIG. 7.—The ratio of the dynamical age of planetary nebulae to the interflash period (i.e., the interval between He shell flashes) of the central stars, as a function of CSPN core mass for the objects in our combined sample. The small value of this ratio argues against the "born-again" hypothesis.

which presents our reservations regarding this interpretation of T_{dyn}). Meanwhile, the evolutionary time scale we have adopted—combining the evolutionary models of Schönberner (1983) and Wood and Faulkner (1986) as described in § III*a* above—has its zero point ($t_{evol} = 0$) corresponding to an end of the superwind mass-loss phase at log $T_{eff} = 3.8$. The values we derive for t_{evol}, however, depend critically on this assumed termination of the superwind phase, as is demonstrated by equation (1) for the transition time from the end of the superwind PN ejection to the point at which $T_{eff} = 30{,}000$ K and the CSPN begins to ionize the nebula. Renzini (1981) has correctly pointed out the difficulty in applying this equation to solve for the unknown transition time, owing to the fact that the residual envelope mass (M_{eR}) remaining at the end of the superwind is itself a largely unknown quantity theoretically; we are not able to determine it directly by observing the proto–CSPN at the end of the superwind phase.

We are therefore left to speculate, as have Renzini (1981) and Iben and Renzini (1983), about CSPNs having long transition times caused by increased values of M_{eR}, due to a premature end to the superwind PN ejection process. But recall that Schönberner (1983) argues against treating M_{eR} as a completely free parameter, citing the hydrodynamical pulsation studies of Härm and Schwarzschild (1975) and Tuchman, Sack, and Barkat (1979), which indicate that the pulsational instability thought to feed the mass-loss process dies out when M_e falls below $\sim 10^{-3}\ M_\odot$. We note, however, that Schönberner's own criteria for defining the t_{evol} zero point, which we have adopted heretofore as well with only a slight modification to couple his models with those of Wood and Faulkner (1986), is based upon the post–AGB models reaching a specific T_{eff} independent of core mass and not upon reaching a critical M_{eR} as a function of core mass.

With this preface, we can now address our third option for resolving the t_{evol} versus t_{dyn} time scale disagreement, noting that the nebular age estimates may provide the key piece of additional information necessary to solve equation (1) with its two unknowns, t_{tr} and M_{eR}. Our approach here is a strictly empirical one, in which we consider the following question: Given that the values adopted for the transition time of each CSPN are uncertain owing to the unknown residual envelope mass (M_{eR}) remaining when the superwind ceases, does one derive reasonable *empirical* residual envelope masses (here denoted M'_{eR}) by requiring that the transition times be such that the t_{evol} match the observed t_{dyn} of the surrounding nebulae?

We chose to derive the empirical residual envelope mass estimates M'_{eR} necessary to answer this question without repeating the model calculations themselves by adopting a series of simplifying assumptions. First, the envelope mass at log $T_{eff} = 3.8$ (here denoted M_{eR_0}) as a function of core mass is determined by interpolating between data published along with the evolutionary models of Schönberner (1983) and Wood and Faulkner (1986); note that we assume these evolutionary models yield the correct envelope mass M_{eR_0} at log $T_{eff} = 3.8$ in the derivation of M'_{eR} which follows. The empirical residual envelope mass which would result were the superwind to end at time t' instead of t_0 is thus:

$$M'_{eR} = M_{eR_0} + \int_{t_0}^{t'} \dot{M}_e\, dt, \tag{3}$$

where $\dot{M}_e$ is the rate of change of envelope mass due to both nuclear burning and surface mass loss *after the superwind has ceased* and is a function not only of time but also of CSPN core mass. By the above definition of M_{eR_0}, t_0 corresponds to $t_{evol} = 0$ and t' corresponds to evolutionary time ($t_{evol} - t_{dyn}$). For $t' < 0$ (i.e., observed values of $t_{dyn} > t_{evol}$), the lack of evolutionary models as functions of time prior to log $T_{eff} = 3.8$ without superwinds forces us to make the simplifying assumption that $\dot{M}_e(t)$ is a constant, here denoted $\dot{M}_0 = \dot{M}_n + \dot{M}_w$ as the sum of constant nuclear burning and wind loss rates, for

$t_{evol} < 0$. Equation (3) therefore becomes

$$M'_{eR} \simeq M_{eR_0} - \dot{M}_0(t_{dyn} - t_{evol}) \; ; \quad t_{dyn} > t_{evol} \; . \tag{4}$$

Equation (4) demonstrates how the constant rate at which the envelope mass decreases ($\dot{M}_0 < 0$) determines how much empirically deduced "additional" residual envelope mass ($M'_{eR} - M_{eR_0}$) is consumed during the extra interval ($t_{dyn} - t_{evol}$) required to reconcile the two time scales; equation (4) applies only to those object where we find "old" nebulae around "young" central stars. We shall later return to objects having $t_{evol} > t_{dyn}$ to derive M'_{eR} from equation (3) by another approach.

Following Schönberner (1983), values of $\dot{M}_0$ were calculated assuming that the mass loss from the stellar surface *after* the superwind ceases is given by the Reimers rate:

$$\dot{M}_w = -4 \times 10^{-13} \, M_\odot \, \mathrm{yr}^{-1} \, \eta \left(\frac{L_*}{g R_*} \right) \tag{5}$$

(Reimers 1975; Kudritzki and Reimers 1978), with the parameter $\eta \sim 1$ and the remaining parameters in solar units. Substituting $g = GM/R_*^2$ and expressing R_* in terms of L_* and T_{eff} in solar units, we can rewrite equation (5) as follows:

$$\dot{M}_w = -4 \times 10^{-13} \, M_\odot \, \mathrm{yr}^{-1} \, \eta \left(\frac{L_*^{3/2}}{M_* \, T_{eff}^2} \right) . \tag{6}$$

Meanwhile, the rate $\dot{M}_n$ at which the envelope mass decreases due to nuclear burning follows from the value of L_* for each CSPN model and the conversion factor 6×10^{18} ergs per gram of hydrogen consumed given by Iben and Renzini (1983). When converted into appropriate units, this implies:

$$\dot{M}_n = -1 \times 10^{-11} \, M_\odot \, \mathrm{yr}^{-1} \, X_e \left(\frac{L_*}{L_\odot} \right) , \tag{7}$$

where X_e is the mass fraction of hydrogen in the CSPN envelope (here set equal to 0.72 based on the nominal value $y = 0.09$ we find from our model atmosphere analysis of CSPN). The net rate of envelope mass consumption ($\dot{M}_0$) then follows from the sum of $\dot{M}_w$ and $\dot{M}_n$, both evaluated at $t_{evol} = 0$. Figure 8 plots this $\dot{M}_0$ sum as a thick line along each of the model tracks used here (see Fig. 1 of Schönberner 1983); the thin straight lines in Figure 8 show $\dot{M}_w$ for each of the CSPN models based on equation (6), in which L_* and M_* are essentially constant during the horizontal phase of evolution in the H-R diagram, leaving $\dot{M}_w$ with only a T_{eff}^{-2} dependence; finally, the dashed lines represent $\dot{M}_n$ for each model based on equation (7), and hence these behave exactly as does L_* as a function of T_{eff}. Compare Figure 8 to Figure 1 of Schönberner (1983).

Note from Figure 8 that the $\dot{M}_w$ component of $\dot{M}_0$ increases with decreasing T_{eff} backward in time along the model tracks. Were the simplifying assumption of constant $\dot{M}_0$ for $t_{evol} \leq 0$ to be dropped in favor of a detailed evolutionary calculation progressing backward in time from log $T_{eff} = 3.8$ in the absence of a superwind, the residual envelope mass required to reconcile the observed t_{dyn} and t_{evol} ages would therefore be greater than the simple empirical estimate M'_{eR} derived on the basis of equation (4), in which we have assumed $\dot{M}_0$ is a constant.

Returning briefly to equation (3) for the few objects in our sample having $t_{evol} > t_{dyn}$, we note that this equation in effect duplicates the model calculations of Schönberner (1983) and Wood and Faulkner (1986) for CSPN evolution to hotter temperatures from log $T_{eff} = 3.8$ (t_0 corresponds to $t_{evol} = 0$; t' corresponds to $t_{evol} - t_{dyn}$ and is here greater than zero, resulting in a superwind which ceases at a higher temperature than log $T_{eff} = 3.8$). We therefore need not repeat these model calculations in order to determine M'_{eR}; equation (3) implies that the superwind in this case continues until the theoretical

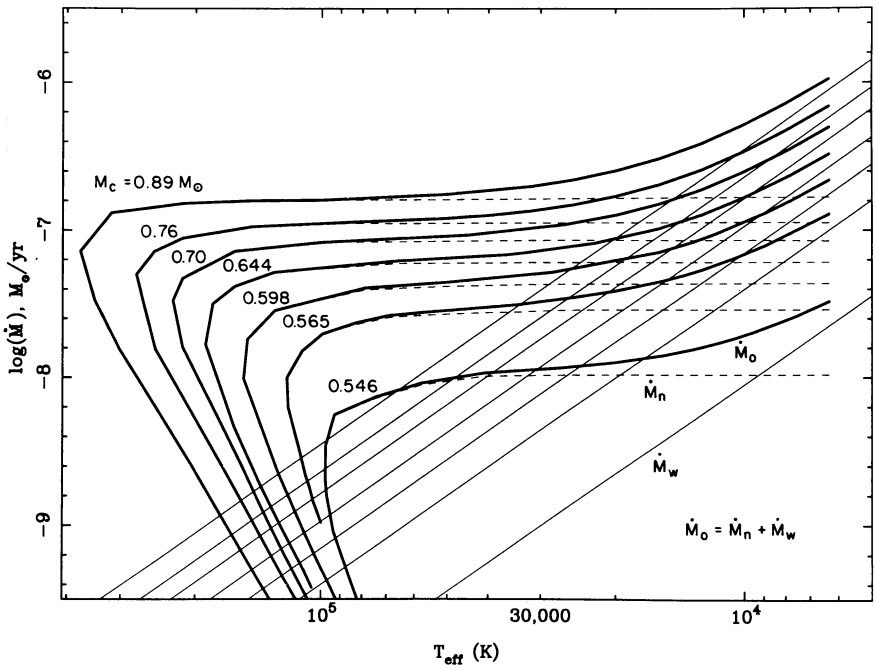

FIG. 8.—Net rate at which a CSPN consumes its envelope mass via nuclear burning (*dashed lines*) and mass loss in a Reimer's wind from the surface (*thin lines*), along the evolutionary models of Schönberner (1983) and Wood and Faulkner (1986). Our concern is with $\dot{M}$ for effective temperatures less than log $T_{eff} = 3.8$, which we assume to be constant for simplicity.

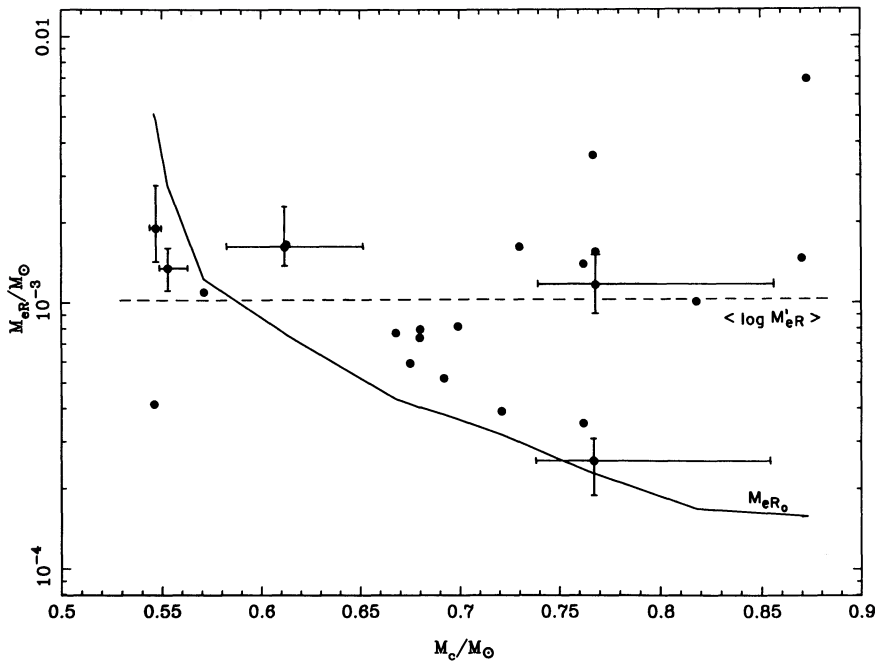

FIG. 9.—Empirical residual envelope masses necessary to reconcile the dynamical and evolutionary time scales for each of the objects in our combined sample (representative error bars are shown for observational data from McCarthy 1988) as a function of CSPN core mass. Solid line shows the residual envelope masses which result from the assumption that the superwind ceases at log $T_{\rm eff} = 3.8$ (see Schönberner 1979, 1983; Wood and Faulkner 1986); dashed line shows the average value of log $M'_{\rm eR}$ we find for our combined sample.

model evolutionary time given by $t' = t_{\rm evol} - t_{\rm dyn}$. Thus, our empirical residual envelope mass is simply

$$M'_{\rm eR} = M_{\rm e}(t') \; ; \quad t_{\rm evol} > t_{\rm dyn} \; , \tag{8}$$

which can be determined directly from the published models (see especially Fig. 3 of Schönberner 1983), because $M_{\rm e}$ is a well-established function of effective temperature and hence evolutionary time beyond the log $T_{\rm eff} = 3.8$ zero point.

Figure 9 shows the results of these empirical residual envelope mass calculations for each CSPN in our combined sample. The points in this figure, which in most cases are lower limits to $M'_{\rm eR}$ as pointed out above for $t_{\rm dyn} > t_{\rm evol}$, fall below $10^{-2}\ M_\odot$ over the entire range of CSPN masses spanned by our sample and do not differ by an implausible amount from the $M_{\rm eR_0}$ values assumed by Schönberner (1983) and Wood and Faulkner (1986). The solid line in Figure 9 shows the residual envelope mass, $M_{\rm eR_0}$, at log $T_{\rm eff} = 3.8$ from these evolutionary models. Therefore, it would seem entirely possible that the poorly understood superwind mass-loss phase ends with a residual envelope mass $M'_{\rm eR}$ *instead of* $M_{\rm eR_0}$ as adopted by the evolutionary theorists on the basis of their $t_{\rm evol} = 0$ at log $T_{\rm eff} = 3.80$ (or 3.75) constraint on this transition phase.

d) Discussion

The results of our numerical experiment simulating the photoionization of an ejected AGB envelope suggested that the expansion rate of the ionization front can indeed exceed that of the bulk material. The question remained, however, To what extent do our simple photoionization models resemble real planetary nebulae? Recall that the possible absorption of Lyman continuum photons by dust was ignored in our model calculations; Spergel, Giuliani, and Knapp (1983) calculated the photoionization of AGB envelopes with and without dust using the CSPN models of Paczyński (1971). They found differences of at most a factor of 2 in the time required to completely ionize a surrounding envelope of a specific mass (selected based on the CO emission results of Knapp *et al.* 1982) and hence also a specific outer radius. Our results based on equation (2) are in general agreement with their "no dust" results, apart from differences in the assumed CSPN evolutionary time scales (note the questionable evolutionary time scales of the Paczyński models owing to an early helium shell flash, as pointed out by Iben and Renzini 1983). Therefore, we conclude that dust absorption will not alter the behavior of our simple photoionization models sufficiently to rule out this possible explanation of the $t_{\rm evol}$ versus $t_{\rm dyn}$ time scale disagreement.

Potentially more serious is that our derivation of equation (2) considered only photoionization of an ejected AGB envelope having a fixed radial density profile $n(r)$. For simplicity, we neglected the probable compression of the AGB envelope into a uniform density shell ($n(r) = \langle n \rangle$, $R_i < r < r_s$) due to the expansion of the $T_e \sim 10^4$ K ionized volume and/or a fast wind from the CSPN (see Kwok, Purton, and FitzGerald 1978; Giuliani 1981; Kwok 1983; Schmidt-Vogt and Köppen 1987*a*, *b*). Thus, while our simple numerical experiments do succeed in demonstrating how it is possible to produce large, low-bulk $v_{\rm exp} \sim V_{\rm ej}$ ionized shells—for which one would calculate "old" $t_{\rm dyn} = r_s/v_{\rm exp}$—around young planetary nebulae central stars, more detailed calculations will be required in order to determine if in fact real planetary nebulae behave in a manner similar to these model ionized AGB envelopes. At present, our rapid photoionization model remains a possible contributing factor to the presence of "old" planetary nebulae around "young" central stars.

Our investigation of the second possibility, that the CSPNs have undergone a late He shell flash, resulted in Figure 7 above and the suggestion that the uppermost objects in this figure (NGC 7293, NGC 1360, and NGC 4361) should be examined

for additional evidence of a late He shell flash, although this mechanism, if it operates at all, would make the time scale disagreement even worse for these low-mass objects having $t_{evol} > t_{dyn}$ already. Here we wish to draw attention instead to the large number of objects in Figure 7 with very small values of the $t_{dyn}/\Delta t_{flash}$ ratio. Since these objects all share the more common $t_{dyn} > t_{evol}$ time scale disagreement, the possible "born-again" experience is a very unlikely explanation of this disagreement for the majority of CSPNs in our sample. Furthermore, as we have pointed out before (Mendez *et al.* 1988), we find a predominance of "old" nebulae around "young" central stars regardless of the temperature of the central star; according to the time scales along the evolutionary tracks calculated by Iben (1984) for such "born-again" CSPNs, they would tend to be observed predominantly at high values of T_{eff}. Hence we conclude that, while helium shell flashes may alter the evolution of a small fraction of CSPNs in our sample, the majority of the "old" nebulae around "young" central stars in Figure 1 must be explained by some other mechanism.

In addition to the high S/N requirements restricting our sample to relatively bright CSPNs, the NLTE model atmospheres we have used to date have been calculated assuming hydrostatic equilibrium. Thus, our sample has been restricted to CSPNs having absorption-line (sd O-type) spectra. The advent of nonhydrostatic model atmospheres (Puls 1988; Gabler *et al.* 1989) will allow us to begin the similarly distance-independent model atmosphere analysis of the Wolf-Rayet (WR–type) CSPNs, many of which show evidence of being H-deficient (Mendez *et al.* 1986) and may have very different evolutionary histories.

The third possible explanation we considered above was that the superwind mass-loss phase might very well come to an end leaving behind a residual envelope mass different than that assumed by either Schönberner (1983) or Wood and Faulkner (1986) in their evolutionary model calculations. Adopting an empirical approach, we were able to derive estimates (M'_{eR}; see Fig. 9) of the theoretically unknown residual envelope masses M_{eR} on which the transition times depend according to equation (1). The implications of these results for the t_{evol} versus t_{dyn} time scale disagreement are the following: the slight additional residual envelope mass we infer for most CSPNs from the difference $(M'_{eR} - M_{eR_0})$ is all that is required to reconcile the evolutionary and dynamical time scales, assuming for the moment that t_{dyn} is correct (at the close of this section, we will reconsider the customary definition of t_{dyn}). By this view, the "old" planetary nebulae are indeed old, and the "young" central stars are older than the Schönberner (1983) and Wood and Faulkner (1986) evolutionary time scales suggest, owing to the extra transition time required to consume the additional residual envelope mass $(M'_{eR} - M_{eR_0})$ we derive on the basis of equation (4).

Note further that for the few low-mass central stars in which originally $t_{evol} > t_{dyn}$, equation (3), equation (8), and Figure 9 suggest that the residual envelope mass at the end of the superwind mass-loss phase is actually slightly less than the value of M_{eR_0} assumed in the model calculations. As a consequence of the inverse relationship between envelope mass and effective temperature (shown explicitly in Fig. 3 of Schönberner 1983), these low-mass central stars would evolve more rapidly than previously believed toward higher temperatures if the superwind carries away a greater amount of their envelope mass (McCarthy 1988).

Evidence that low-mass CSPNs may indeed evolve quickly to high T_{eff} comes not only from the sample of nebulae studied by Gathier (1984), which as we mentioned in § III*c* above may be dominated by central stars many times *older* than their surrounding nebulae, but also from a previous observation of ours (Mendez *et al.* 1988) that we find a curious absence of low-mass, low-T_{eff} central stars in our distance-independent study of CSPNs. While this may be a selection effect, given the small size of our sample at present (23 CSPNs) and our bias toward more luminous, and therefore more massive, central stars, we note that the difference in visual magnitude M_V between 0.8 and 0.55 $M_\odot$ central stars at $T_{eff} = 30{,}000$ K is small compared to the difference in visual magnitude M_V owing to the bolometric correction between 30,000 K and 100,000 K ($\Delta M_V = 2^m.5$ and $4^m.0$, respectively). Since our sample does include four CSPNs with masses less than 0.6 $M_\odot$ and $T_{eff} \geq 65{,}000$ K, the fact that we find no such objects in our sample with $T_{eff} < 65{,}000$ K suggests a genuine absence of low-mass, low-T_{eff} CSPNs and lends support to the contention that these low-mass central stars evolve quickly to high T_{eff} as a result of their superwind mass-loss phases continuing beyond log $T_{eff} = 3.8$. This contention is examined by Gathier and Pottasch (1989), who also consider the possibility that greater post-superwind mass-loss rates may be responsible for speeding the evolution of low-mass CSPNs toward higher effective temperatures (see also Trams *et al.* 1989).

It is worthwhile to consider once again the theoretical basis for the solid line representing M_{eR_0} as a function of core mass M_c in Figure 9. It arises from the constraint, imposed by Schönberner (1983) and Wood and Faulkner (1986) in their evolutionary calculations, that the superwind phase ends at a single specific temperature independent of core mass (see § III*a* for details). But the pulsational studies (Härm and Schwarzschild 1975; Tuchman, Sack, and Barkat 1979) on which this transition temperature is assigned studied only a very narrow range of core masses (0.62–0.68 $M_\odot$; critical envelope masses 1.0×10^{-3}–1.4×10^{-3} $M_\odot$). While this does in fact lead to a transition temperature between log $T_{eff} = 3.7$ and 3.8 for a 0.65 $M_\odot$ CSPN, we do not agree with the assumption that this same transition temperature must therefore apply to all CSPNs regardless of core mass. Unfortunately, the mechanisms responsible for the superwind phase itself are poorly understood at present; specifying precisely when the superwind phase ceases for all CSPN masses cannot therefore be done theoretically with any confidence on the basis of just the Härm and Schwarzschild (1975) or Tuchman, Sack, and Barkat (1979) results alone.

Our empirical residual envelope masses span the range of core masses from 0.546 to 0.87 $M_\odot$ found in our sample of CSPNs. Note that the scatter of M'_{eR} at a given core mass in Figure 9 is large; a linear or quadratic least-squares fit through these points has little significance, being influenced mainly by the outlying points. The distribution is therefore best described by a constant value of M_{eR} independent of core mass, and we have indicated this value as a horizontal dashed line through Figure 9 to contrast it with the theoretical M_{eR_0} curve resulting from the log $T_{eff} = 3.8$ constraint. The implication of a constant M_{eR} for all core masses is illustrated in Figure 10 (adapted from Fig. 3 of Schönberner 1983); from this figure, it is clear that low-mass central stars must evolve quickly to high temperatures if the superwind continues until a residual mass of $\sim 10^{-3}$ $M_\odot$ is reached. If the absence of low-mass CSPNs at low effective temperatures remains as our sample increases in size, we would interpret this as strong evidence against the

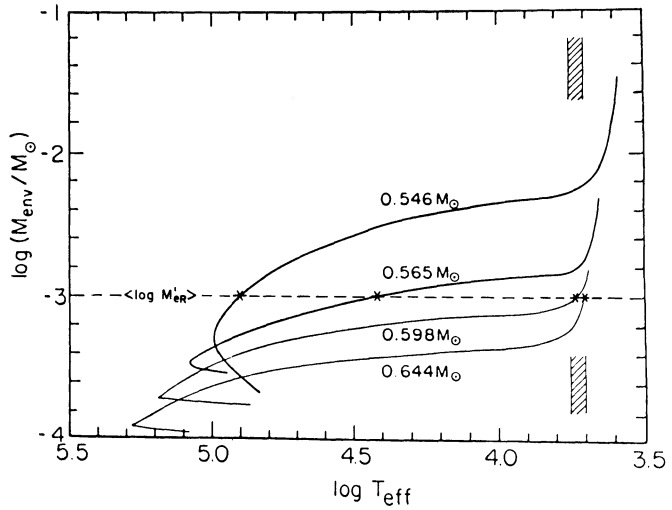

FIG. 10.—Our average value of log M'_{eR} shown in the context of Fig. 3 of Schönberner (1983), relating the decrease in CSPN envelope mass to the increase in T_{eff} which results. Asterisks (*) show the temperature to which CSPNs would evolve were the superwind to continue until $M_e = 10^{-3}\ M_\odot$ is reached; note that low-mass CSPNs would evolve quickly to high effective temperature were this to occur.

assumed M_{eR_0} curve in Figure 9 and in favor of a more constant M_{eR} behavior with core mass, such as that implied by the empirical residual envelope mass distribution.

Finally, it is important to stress that throughout this paper we have considered each of the three possibilities for explaining the disagreement between t_{dyn} and t_{evol} shown in Figure 1 *independently* of the other two possibilities. In particular, we wish to stress that the empirical residual envelope masses (M'_{eR}) were derived above on the assumption that the customary t_{dyn} estimates represent the dynamical ages of the surrounding planetary nebulae, and we found that the additional envelope masses ($M'_{eR} - M_{eR_0}$) needed to reconcile the evolutionary and dynamical time scales were not unreasonably large (i.e., all our $M'_{eR} < 10^{-2}\ M_\odot$). On this basis, we were unable to rule out a premature end to the superwind phase as an explanation for the time scale disagreement. Note the distinction between this conclusion and the claim that our M'_{eR} empirical residual envelope mass estimates in Figure 9 are "correct"; for reasons we will discuss below, there is reason to treat them as upper limits to M_{eR}, which in fact strengthens the argument in favor of this explanation as a means of reconciling the time scale disagreement.

The reason why the M'_{eR} empirical residual envelope masses are likely to be overestimates of the true M_{eR} stems from our use of the customary definition of the dynamical ages of the surrounding nebulae, namely $t_{dyn} = r_s/v_{exp}$. As we pointed out in § III*b* above and emphasize here at the recommendation of an anonymous referee, the use of outer nebular radii (r_s) instead of inner radii (R_i) leads to a value of t_{dyn} greater than the time since the *end* of the superwind phase. We then overestimate M_{eR} when we derive M'_{eR} according to equation (4). There are unfortunately only a few planetary nebulae in our sample for which we can determine the ratio of R_i/r_s from the literature (these are listed in Table 2). For the remainder, it is necessary to consider models of the expected behavior of the ratio R_i/r_s as the nebula expands; both Phillips (1984) and Taylor, Pottasch, and Zhang (1987), have suggested that the fractional shell thickness of a planetary nebula ($1 - R_i/r_s$) is expected to

TABLE 2

INNER/OUTER RADII RATIOS FOR INDIVIDUAL NEBULAE

Object (1)	R_i/r_s (2)	Reference (3)
NGC 7293	0.68	Phillips 1984
A 36	0.70	Perek and Kohoutek 1967
NGC 1535	0.40	Chu 1989
NGC 3242	0.30	Phillips 1984
NGC 7009	0.54	Phillips 1984
NGC 6629	0.45	Taylor, Pottasch, and Zhang 1987
NGC 6891	0.50	Phillips 1984
IC 418	0.31	Taylor, Pottasch, and Zhang 1987
He 2–108	0.83	Henize 1967

increase as the nebula expands. Figure 11 presents the combined samples of these two nebular studies on the same plot (note that Phillips tabulated his measurements in terms of $\Delta R/d = (r_s - R_i)/2r_s$, which we have transformed into $R_i/r_s = 1 - 2(\Delta R/d)$ for purposes of this discussion). We feel that there is little justification for fitting a model curve through the points in Figure 11 given the amount of scatter in the diagram; although the ordinate of the plot, R_i/r_s, is distance independent, the abscissa depends on the angular radii of the nebula and the (rather uncertain) assumed distance. We would therefore choose to simply adopt the average value, $\langle R_i/r_s \rangle = 0.43$, for the remaining objects in our sample not found in Table 2.

Note that the ratio of inner to outer nebular radii span a range from 0.3 to 0.8—with an average value of 0.5—for the objects in our sample with measureable inner radii (Table 2). This is consistent with Figure 11, given the small number of nebulae in Table 2; the major selection effect expected would favor nebulae with large radii, having perhaps smaller values of R_i/r_s. Hence, a refined set of residual mass estimates can be derived from Table 1 by applying the correction, $M_{eR} = (R_i/r_s)(M'_{eR} - M_{eR_0})$. As a result of this first-order correction, the points above the solid line in Figure 9 will move roughly halfway in the direction of the solid line representing M_{eR_0}. However, we believe that this first-order correction is still insufficient to yield "correct" residual mass estimates, because the definition of $t_{dyn} = R_i/v_{exp}$ still neglects the detailed dynamics of an expanding planetary nebula shell (e.g., the interaction between the slow superwind ejecta and a fast wind from the young central star, which is thought to increase v_{exp} with time). Lastly, recall that in our derivation of equation (4) above we assumed a constant mass-loss rate $\dot{M}_0$ for $t_{evol} \leq 0$; Figure 8 clearly suggests that this assumption must be dropped in order to derive "correct" empirical residual envelope masses, because equation (4) will lead to underestimates of the true M_{eR}. In the end, an accurate picture of the AGB star to planetary nebula transition will require that we abandon both our simplifying constraints on the end of the superwind phase and our simple models of the subsequent expansion of planetary nebulae.

V. CONCLUSIONS

We have derived estimates of the CSPN residual envelope mass remaining at the end of the superwind AGB mass-loss phase using an empirical approach based on the additional time scale information provided by the dynamical expansion of the surrounding planetary nebulae. We believe that the disagreement between our derived evolutionary and dynamical ages are due to departures of the residual envelope masses

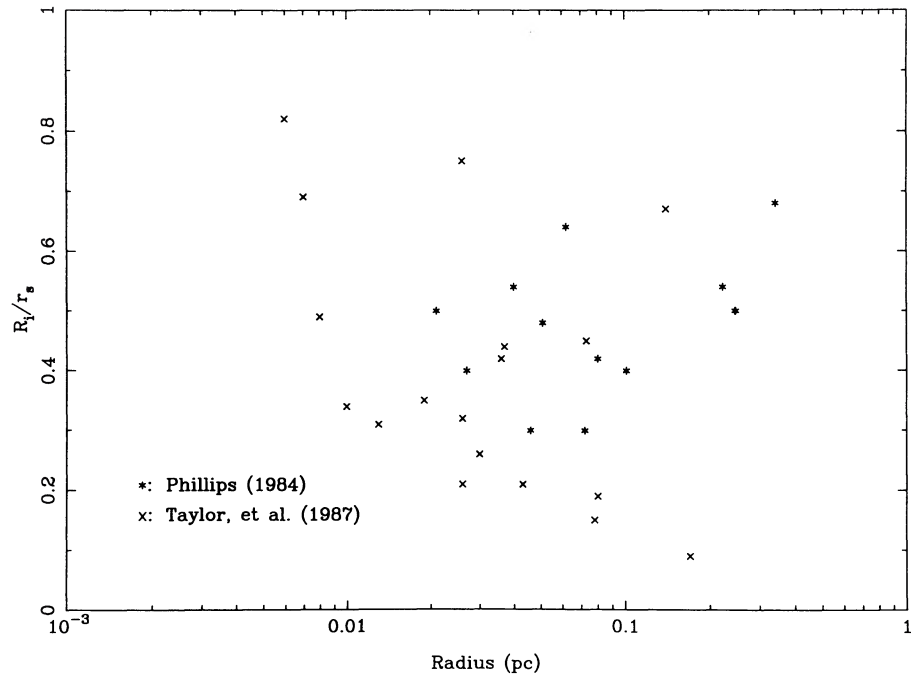

FIG. 11.—Ratio of planetary nebulae inner to outer radii as a function of the outer radii, taken from the work of Phillips (1984) and Taylor, Pottasch, and Zhang (1987). Note the large scatter; only the R_i/r_s ordinate is distance independent.

from those predicted on the basis of a temperature constraint governing the end of the superwind phase; our technique for determining empirical residual envelope masses may be an important step toward a better understanding of the superwind mass-loss mechanism and the transition from the AGB star to planetary nebula phases of stellar evolution. However, the possible effects on the dynamical time scale due to the rapid photoionization of ejected material need to be better understood before more accurate empirical envelope mass estimates can be derived; a well-determined set of nebular shell inner radii used instead of outer radii would also improve upon our existing dynamical age estimates. Finally, we have shown that the time scale disagreement present in our sample cannot have its origin entirely in the late He shell flash hypothesis, although our sample does not at present include any WR–type CSPNs which, being hydrogen deficient, may have quite different evolutionary histories.

We wish to acknowledge the very generous telescope time allocations we have received to conduct our echelle observations of CSPNs, both at the ESO 3.6 m and Palomar 1.5 m telescopes. J. K. M. would like to thank Commission 38 of the IAU for a travel grant to Munich where this fruitful international collaboration was begun. This work was supported in part by grant ASP 85-02518 from the N.S.F. to J. R. M., and by grant Ku 474/8-2 from the Deutsche Forschungsgemeinshaft to R. P. K. R. H. M. would like to thank the Alexander von Humboldt Foundation of West Germany for a research fellowship at the Institut für Astronomie und Astrophysik der Universität München, as well as the Max-Planck-Institut Astrophysik, Garching bei München, for additional support. A. H. is grateful for an external fellowship from the European Space Agency. Finally, we wish to thank an anonymous referee for suggestions which resulted in a clearer presentation and a better paper.

REFERENCES

Acker, A. 1978, *Astr. Ap. Suppl.*, **33**, 367.
Acker, A., Gleizes, F., Chopinet, M., Marcout, J., Ochsenbein, F., and Roques, J. M. 1982, *Catalogue of Central Stars of True and Possible Planetary Nebulae* (Publication Spéciale du C.D.S. N° 3) (Strasbourg: Observatoire de Strasbourg).
Bohuski, T. J., and Smith, M. G. 1974, *Ap. J.*, **193**, 197.
Cahn, J. H., and Kaler, J. B. 1971, *Ap. J. Suppl.*, **22**, 319.
Chu, Y.-H. 1989, in *IAU Symposium 131, Planetary Nebulae*, ed. S. Torres-Peimbert (Dordrecht: Reidel), p. 105.
Cudworth, K. M. 1974, *A.J.*, **79**, 1384.
Daub, C. T. 1982, *Ap. J.*, **260**, 612.
D'Odorico, S., Enard, D., Lizon, J. L., Ljung, B., Nees, W., Ponz, D., Raffi, G., and Tanné, J.-F. 1983, *ESO Messenger*, **33**, 2.
Gabler, R., Gabler, A., Kudritzki, R. P., Puls, J., and Pauldrach, A. 1989, *Astr. Ap.*, in press.
Gathier, R. 1984, Ph.D. thesis, University of Gronigen.
Gathier, R., and Pottasch, S. R. 1989, *Astr. Ap.*, **209**, 369.
Giuliani, J. L. 1981, *Ap. J.*, **245**, 903.
Härm, R., and Schwarzschild, M. 1975, *Ap. J.*, **200**, 324.
Henize, K. G. 1967, *Ap. J. Suppl.*, **14**, 125.
Herrero, A. 1987*a*, *Astr. Ap.*, **171**, 189.
———. 1987*b*, *Astr. Ap.*, **186**, 231.
Iben, I. 1984, *Ap. J.*, **277**, 333.
Iben, I., Kaler, J. B., Truran, J. W., and Renzini, A. 1983, *Ap. J.*, **364**, 605.
Iben, I., and Renzini, A. 1983, *Ann. Rev. Astr. Ap.*, **21**, 271.
Knapp, G. R., Phillips, T. G., Leighton, R. B., Lo, K.-Y., Wannier, P. G., Wootten, H. A., and Huggins, P. J. 1982, *Ap. J.*, **252**, 616.
Kudritzki, R. P., and Mendez, R. H. 1989, in *IAU Symposium 131, Planetary Nebulae*, ed. S. Torres-Peimbert (Dordrecht: Reidel), p. 273.
Kudritzki, R. P., and Reimers, D. 1978, *Astr. Ap.*, **70**, 227.
Kwok, S. 1983, *Ap. J.*, **258**, 280.
Kwok, S., Purton, C. R., and FitzGerald, M. P. 1978, *Ap. J.* (*Letters*), **219**, L125.
le Luyer, M., Melnick, J., and Richter, W. 1979, *ESO Messenger*, **17**, 27.
Masson, C. R. 1989, *Ap. J.*, **336**, 294.
McCarthy, J. K. 1988, Ph.D. thesis, California Institute of Technology.
Mendez, R. H., Kudritzki, R. P., Gruschinske, J., and Simon, K. P. 1981, *Astr. Ap.*, **101**, 323.

Mendez, R. H., Kudritzki, R. P., and Simon, K. P. 1983, in *IAU Symposium 103, Planetary Nebulae*, ed. D. R. Flower (Dordrecht: Reidel), p. 343.
———. 1985, *Astr. Ap.*, **142**, 289.
Mendez, R. H., Kudritzki, R. P., Herrero, A., Husfeld, D., and Groth, H. G. 1988, *Astr. Ap.*, **190**, 113.
Mendez, R. H., Miguel, C. H., Heber, U., and Kudritzki, R. P. 1986, in *Hydrogen Deficient Stars and Related Objects*, ed. K. Hunger, D. Schönberner, and N. Kameswara Rao (Dordrecht: Reidel), p. 323.
Paczyński, B. E. 1971, *Acta Astr.*, **21**, 47.
———. 1975, *Ap. J.*, **202**, 558.
Perek, L., and Kohoutek, L. 1967, *Catalogue of Galactic Planetary Nebulae* (Praha: Academia Press, CSSR).
Phillips, J. P. 1984, *Astr. Ap.*, **137**, 92.
Puls, J. 1988, *Astr. Ap.*, **184**, 227.
Reimers, D. 1975, *Mem. Soc. Roy. Sci. Liege*, **8**, 369.
Renzini, A. 1981, in *Physical Processes in Red Giants*, ed. I. Iben and A. Renzini (Dordrecht: Reidel), p. 431.
Schmidt-Vogt, M., and Köppen, J. 1987*a*, *Astr. Ap.*, **174**, 211.
———. 1987*b*, *Astr. Ap.*, **174**, 223.
Schönberner, D. 1979, *Astr. Ap.*, **79**, 108.
———. 1981, *Astr. Ap.*, **103**, 119.
———. 1983, *Ap. J.*, **272**, 708.
Shklovskiĭ, I. S. 1956, *Soviet Astr.—AJ*, **33**, 315.
Spergel, D. N., Giuliani, J. L., and Knapp, G. R. 1983, *Ap. J.*, **275**, 330.
Spitzer, L. 1978, *Physical Processes in the Interstellar Medium* (New York: Wiley).
Strömgren, B. 1939, *Ap. J.*, **89**, 526.
Taylor, A. R., Pottasch, S. R., and Zhang, C. Y. 1987, *Astr. Ap.*, **171**, 178.
Trams, N. R., Waters, L. B. F. M., Waelkens, C., Lamers, H. J. G. L. M., and van der Veen, W. E. C. J. 1989, *Astr. Ap.*, **218**, L1.
Tuchman, Y., Sack, N., and Barkat, Z. 1979, *Ap. J.*, **234**, 217.
Westerlund, B. E., and Henize, K. G. 1967, *Ap. J. Suppl.*, **14**, 154.
Wilson, O. C. 1950, *Ap. J.*, **111**, 279.
Wood, P. R. 1979, *Ap. J.*, **227**, 220.
Wood, P. R., and Faulkner, D. J. 1986, *Ap. J.*, **307**, 659.

H. G. GROTH, D. HUSFELD, and R. P. KUDRITZKI: Institut für Astronomie und Astrophysik der Universität München, Universitäts Sternwarte, Scheinerstrasse 1, 8000 München 80, West Germany

A. HERRERO: Instituto de Astrofisica de Canarias, 38200 La Laguna, Tenerife, Spain

J. K. McCARTHY: Department of Astronomy, RLM 15.308, University of Texas at Austin, Austin, TX 78712

R. H. MENDEZ: Instituto de Astronomia y Fisica del Espacio, C.C. 67, 1428 Buenos Aires, Argentina

J. R. MOULD: Department of Astronomy, M/S 105-25, California Institute of Technology, Pasadena, CA 91125